Measuring the Cortical Thickness

Frithjof Kruggel & D. Yves von Cramon
Max-Planck-Institute of Cognitive Neuroscience
Stephanstraße 1, 04103 Leipzig, Germany
{kruggel,cramon}@cns.mpg.de

Abstract

Besides normal aging, a number of brain diseases are known to reduce the amount of grey matter in the brain. To better understand the nature and progression of these disease processes, quantitative measurements of relevant brain structures, such as the regional cortical thickness, are highly desirable. Starting from high resolution volumetric MR images of the human head, a reliable segmentation procedure for the grey matter compartment is described which allows thickness measurements at sub-voxel resolution. Simulation experiments and comparisons with published data from histological examinations prove the validity of results.

1. Introduction

A thin sheet on the outer surface of both brain hemispheres contain approximately 80% of the neurons of the central nervous system. This so-called neocortex (grey matter, GM) measures only 1.5-4.5 mm [1], but its extent reaches 4000 cm^3, due to the folding (gyrification) of the brain. Strong local connections (0-3 mm) between neurons are formed within this sheet, thus promoting the idea of local "processing units". More remote (20-100 mm) connections are acheived via fibers in white matter (WM) tracts, as either connections between gyri, hemispheres, or between a gyrus and core centers of the brain, the basal ganglia.

A number of factors reduce the amount of grey matter during life. Most notably, a global cortical thinning occurs during aging [9, 16]. Neurodegenerative diseases, such as M. Alzheimer [15] and Chorea Huntington [13], lead to characteristic circumscribed atrophies of the brain, and cognitive disabilities acquired from these diseases may be related to the cell loss in a specific neurofunctional area. For neurobiology, it is highly interesting to study the regional cortical thickness and its variation under the condition of degenerative brain diseases.

T_1-weighted, high-resolution 3D magnetic resonance (MR) scanning offers an easy way to obtain an in-vivo description of the human brain. In fact, an increasing number of clinical studies incorporate recording such volume data with the intent to extract quantitative descriptors for pathological processes from them.

The extraction and description of the neocortical surface has received much interest in the computer vision literature, especially its differential geometric aspects, and far too many references exist to list them here (for an introduction, see [6]). Most surprisingly, very little attention has been paid to the neurobiologically relevant problem of determining the cortical thickness by image processing. To best of our knowledge, only a few very recent references focus on this problem [4, 9, 22], however they do not offer a satisfying solution.

A reliable segmentation of the neocortical layer is considered a non-trivial task. A simple-minded strategy for determining the cortical thickness would use a segmentation of the white matter, apply a distance transform to it, and record the values on the surface of the grey matter as its thickness. However, the partial volume effect found in any brain imaging method leads to fuzzy boundaries between the grey matter and its neighboring compartments, the white matter and to the cerebrospinal fluid (CSF). Thus, a high variance is expected in the results of voxel-based methods. "Sub-voxel" techniques must be applied to warrant neurobiologically meaningful results.

Another problem complicates the segmentation of the grey matter. To a certain extent, all MR imaging protocols are sensitive to inhomogeneities of the B_1 magnetic field, which results in a spatial variation of the image intensity. So care must be taken to correct for these intensity inhomogenities in order to obtain values which are comparable across brain regions and between individuals.

Even if a successful segmentation is obtained, care should be taken to interpret the result as grey matter. The brain is suspended in the skull, and supplying arteries, draining veins and cranial nerves connect the brain to other structures. Unfortunately, especially veins and meninges are hard to discriminate based on intensity criteria, and thus

0-7695-0737-9/00 $10.00 (c) 2000 IEEE

may contribute to the segmented grey matter compartment.

In this paper, we describe an approach to determine the cortical thickness from T_1-weighted, volumetric MR images of the human brain. Because brain atrophies are often circumscribed, we show how the measures are obtained in gyral subcompartments and in relation to the folding characteristics.

2. Algorithms

We now describe our approach for the grey matter segmentation and the measures derived from it. Our procedure is inspired by recent publications of Xu *et al.* [21], Zeng *et al.* [22], and Magnotta *et al.* [9]. Some steps correspond to well-known methods in image processing, so we deliberately keep the description short. Instead, we focus on details considered important for a reliable and fast segmentation procedure.

We used high-resolution, T_1-weighted MR data sets of the human head. First, we visually identified the position of key structures of the stereotactical coordinate system, the anterior and posterior commissure [7]. Then, we performed an affine transformation using b-spline interpolation [18] to yield an aligned data set in an isotropical resolution of 1 mm.

It was necessary to correct for intensity inhomogeneities, which would lead to segmentation errors especially at the GM-WM boundary in small gyral stalks. From the set of proposed methods, we selected the algorithm described by Pham and Prince [11]. It models the image as a set of different materials with different Gaussian-distributed intensity distributions, which are distorted by a spatially smooth, but varying multiplicative background field. A fuzzy c-means classification algorithm is used to determine per-voxel class probabilities, and the background field is recovered regularized by a partial differential equation system. We used the recovered background field to correct intensities in the original data set.

An initial WM segmentation was obtained from the class containing mostly WM voxels in the previous step by removing connections to its outer hulls. Necessary steps were described elsewhere [7]. The brainstem and cerebellum were removed by cutting the brainstem at a level 15 mm below the posterior commissure and selecting the biggest connected component.

The surface of this WM segmentation was computed via the marching tetrahedra algorithm [10], which yielded topologically correct triangulated surface meshes of 500-900 k vertices. This mesh may be simplified by any published method. We applied the "wrapper"-algorithm [5] to acheive an 8-fold reduction of the vertex count.

An improved model of the WM surface was obtained by treating this initial WM surface as a deformable model [17]. With modifications, we follow the ideas of Xu *et al.* [20] and Dale and Sereno [2] here. On any vertex v_0 in the mesh, internal and external forces act until a balance is acheived. The internal force F_{int} tries to center a vertex among its edge-connected neighbors $\{v_i\}_{i=1,N}$:

$$F_{int} = \frac{1}{N}\sum_{i=1}^{N}(v_i - v_0). \tag{1}$$

The first external force $F_{ext,1}$ tears a vertex outwards along the direction of its surface normal n_0. This force is exerted by an intensity-gradient field f, which is computed from a convolution of the intensity-corrected image I with a Gaussian kernel G: $f = \nabla(G \circ I)$ [20]:

$$|F_{ext,1}| = f(v_0) \bullet n_0, \tag{2}$$

where $\bullet$ denotes the inner product. The second external force $F_{ext,2}$ captures the surface within a narrow range around an image intensity I_{lim}:

$$|F_{ext,2}| = \tanh(\kappa\ (I(v_0) - I_{lim})), \tag{3}$$

where κ corresponds to the capturing range and is related to the noise level in the data set. $F_{ext,2}$ pushes a vertex outside until a position with intensity I_{lim} is reached, and inside if the intensity is too low. A suitable value for I_{lim} was chosen as the average of the class center intensities for WM and GM in the initial segmentation step. Forces are weighted to ensure good convergence properties during iterations t of the surface adaption process:

$$\begin{aligned} v_0(t+1) \quad = \quad & v_0(t) + w_1\ F_{int} + \\ & n_0(w_2\ |F_{ext,1}|\ |F_{ext,2}| + w_3\ |F_{ext,2}|). \end{aligned} \tag{4}$$

The image gradient force $|F_{ext,1}|$ is weighted by the intensity force $|F_{ext,2}|$ in order to reduce the outward-driving force adaptively when the destination intensity range is reached. This constraint also reduces the chance of introducing self-intersections. The process is iterated until the sum of vertex position shifts falls below a pre-set limit. The result is kept as the final representation of the WM surface.

We determined local curvature properties of this surface using the coordinate transformation method [14]. To each vertex v_0, a tangential plane is adapted, which is described by its two orthogonal vectors x and y. Each vertex $\{v_i\}_{i=1,N}$ in the local neighborhood is represented by its local coordinates $(x_i, y_i, h(x_i, y_i))$, where $h(\cdot)$ denotes the distance to the plane. A parabolic surface patch $O(x, y) = (x, y, ax^2 + 2bxy + cy^2)$ is adpated to this set of vertices, and the Gaussian curvature $K = 4(ac - b^2)$ and the mean curvature $H = a + c$ are extracted and stored as an attribute of the vertex v_0.

Next, the GM surface was computed from the WM surface by setting I_{lim} to the average intensity of the GM and

CSF class and performing the surface adaption as described above.

The GM thickness was interpreted as the local minimal distance between the GM and the WM surface. This thickness was computed for each vertex as follows: A vertex $v_{0,GM}$ of the GM mesh was projected onto a triangle of the WM mesh along its plane normal. If the projection point $v_{p,WM}$ was found within the triangle, the distance $||v_{0,GM} - v_{p,WM}||$ was determined, and the shortest distance to all triangles was recorded as the cortical thickness at $v_{0,GM}$. A surprisingly large number of different cases had to be discriminated in this apparently simple geometrical problem [3]. In order to avoid the cost of O^2 operations for a brute force search, we implemented a "spatial cache": for each voxel of the volume, we recorded a list of vertices located within this voxel. Since the GM surface originated from the WM surface, a first guess for the closest vertex on the WM mesh is given by the WM vertex $v_{0,WM}$ with the same index as $v_{0,GM}$. We limited the search for the closest projection point to a small subregion around $v_{0,WM}$, guided by the spatial cache, which resulted an approximately linear performance. The cortical thickness was stored as an attribute of vertex $v_{0,GM}$.

Now, a number of options exist to introduce subregions on the cortical surface. Such regions may be defined on the basis of the atlas transformation applied in the beginning. For its simplicity, we preferred a regional segmentation of sulcal substructures, the so-called sulcal basins [8]. Sulci of the WM segmentation were closed by a morphological operation. A constrained distance transform was applied to these sulcal fillings, and local maxima were recorded as the deepest points in the sulci. From these deepest points, a region growing algorithm introduced a segmentation by labelling the neighborhood. Thus, sulcal subregions received different labels and were interpreted as structural entities of the cortex. This label was stored as an attribute of vertex $v_{0,GM}$.

As a result of this procedure, we obtained a triangulated mesh representing the GM surface. At each vertex, we have the position, the normal, the local curvature, the cortical thickness and a region label.

3. Experiments

We conducted a series of experiments to evaluate the preciseness of the measurements, to find suitable ranges for the parameters of this procedure, and to study results in an example normal subject and a patient suffering from clinically diagnosed Alzheimer's disease.

3.1. Accuracy and Precision Using Simulated Data

In order to obtain some information about the preciseness of the measurements under the condition of the partial volume effect, a simulation experiment was conducted. A sphere of intensity $I = 140$ and diameter $d = 80$ voxels was located in a cubic volume of 256^3 voxels of background intensity $I = 20$. A spherical layer of intensity $I = 80$ and varying diameter was placed around the center sphere, simulating the GM compartment. To simulate the partial volume effect, the cube was linearly downscaled by a factor of 4. WM surfaces were computed at $I_{lim} = 110$, GM surfaces at $I_{lim} = 50$. Measured thickness values were compared with the true values in Fig. 1. Except for a distance of 0.5 mm, the difference between the measured and the true distance was less than 1.5 %, with a variance of less than 2 %.

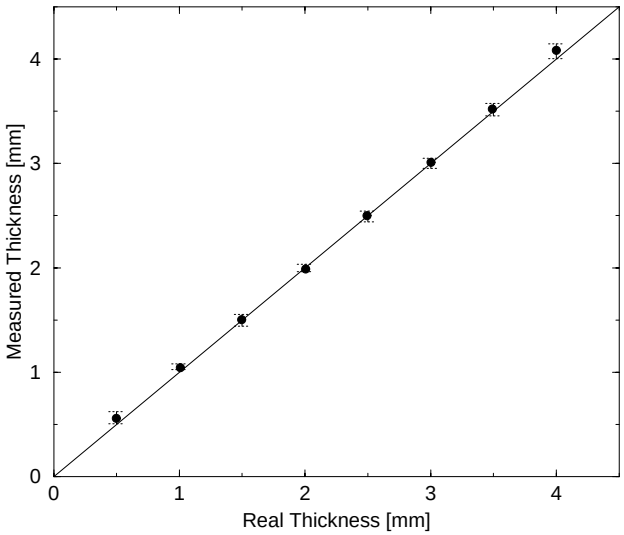

Figure 1. Sphere simulation experiment: Measured mean and variance of the layer as a function of the simulated thickness.

3.2. Parameter Study

The surface adaption algorithm is governed by the intensity limit I_{lim}, the intensity window κ and the weights w_i.

The relative ratio of the weights influence the mode of surface propagation, while the absolute values of w_2 and w_3 determine the propagation speed. From a series of experiments, we found $w_1 = 0.05$, $w_2 = 0.0001$, and $w_3 = 0.01$ as suitable for all studied problems. Convergence was assumed after a fixed number of 500 iterations. The intensity window is related to the noise level of the data set, and $\kappa = 0.3$ was chosen here. Higher values tended to impede convergence, while smaller values produced surfaces which were considered too smooth.

The dependency of the cortical thickness on the intensity limits was studied for a cortical patch from a normal subject. The WM limit was set to values of $\{100, 110, 120, 130, 140\}$ consecutively, and was recorded as a function of the intensity difference $I_{lim,WM} - I_{lim,GM}$. Results were compiled in Fig. 2.

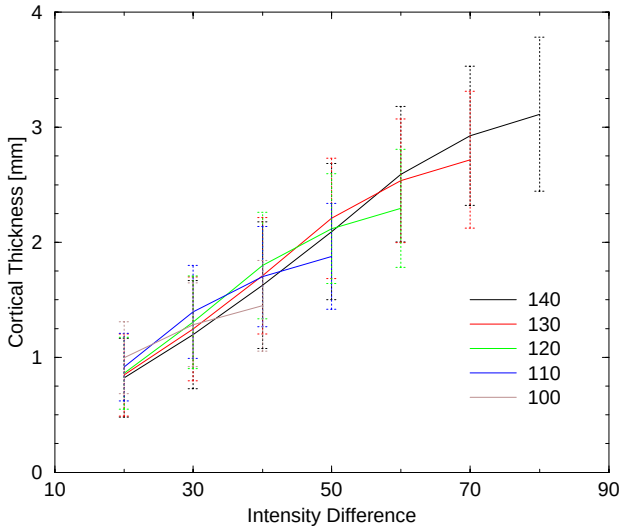

Figure 2. Cortical thickness as a function of the grey matter intensity interval, starting from different white matter border intensities for a sample normal subject. An approximately linear increase of 0.045 mm per intensity unit was found, which is interpreted as a consequence of the partial volume effect.

For the intensity range from 60..140 units in this data set, an almost constant increase in cortical thickness of 0.045 mm per intensity unit was found. This finding was interpreted as a consequence of the partial volume effect, which leads to a continuous intensity falloff across the GM layer. As suggested by Xu *et al.* [21], we selected values for I_{lim}, which corresponded to the crosspoints of the class membership probabilities from the initial segmentation step, e.g. $I_{lim,WM}$ was set to the intensity where $p(WM) = 0.5$ and $p(GM) = 0.5$.

3.3. Examples

As a first example, we selected a MR data set from a normal healthy subject. 128 sagittal T_1-weighted slices of 256^2 voxels were obtained at a spatial resolution of 0.94x0.94x1.5 mm on a Bruker Medspec 100 system at 3.0 T using a MDEFT sequence. Our segmentation procedure was applied to this data set, with $I_{lim,WM} = 120$ and $I_{lim,GM} = 60$. The measured cortical thickness was color-coded on the GM surface (see Fig. 3, next page).

An elderly patient suffering from Alzheimer's disease was chosen as a second example. Here, the data set was recorded on a Siemens Vision system at 1.5 T using a GRE sequence with 128 axial slices of 256^2 voxels at a spatial resolution of 0.97x0.97x1.4 mm. Results are shown as Fig. 4 (next but one page), with $I_{lim,WM} = 140$ and $I_{lim,GM} = 70$ in this case.

In comparison with the normal case, a marked general atrophy was found in fronto-temporal parts of the brain. The parietal and occipital lobe, as well as posterior portions of the temporal lobe appeared relatively unaffected. However, there was a general reduction in the cortical thickness, which was more prominent in the frontal lobes. Thickness measurements in subregions were obtained by examining vertices with certain region labels. Results for neurofunctionally interesting subregions were compiled in Tab. 1 on the next page.

These quantitative measurements underline the qualitative message from Fig. 4: a general reduction of the cortical thickness was found for the patient case, with a strongest reduction in the frontal lobes of ≈40 %. Values for the normal case compared nicely with published data from histological examinations: Middle frontal gyrus: 2.47±0.29 mm [12], inferior frontal gyrus: 2.45±0.28 mm [12], superior temporal gyrus: 2.49±0.10 mm [16], banks of the calcarine sulcus: 1.72±0.18 mm [23]. We assume that the higher variance in our results originated most likely from noise. We determined a noise level of $\sigma = 6.5$ in our MR data sets, leading to an error of ≈0.3 mm on both GM boundaries.

Histological examinations revealed that the cortex at fundi reaches only 50-60 % of the thickness at gyral crowns [1, 19]. Similar ratios were found for an example patch of the frontal cortex in the normal case (see Fig. 5, next but one page). Concave fundus regions (magenta) had a thickness of 1.5..2.0 mm, whereas convex crown regions (yellow-red) a thickness of 2.4-2.8 mm.

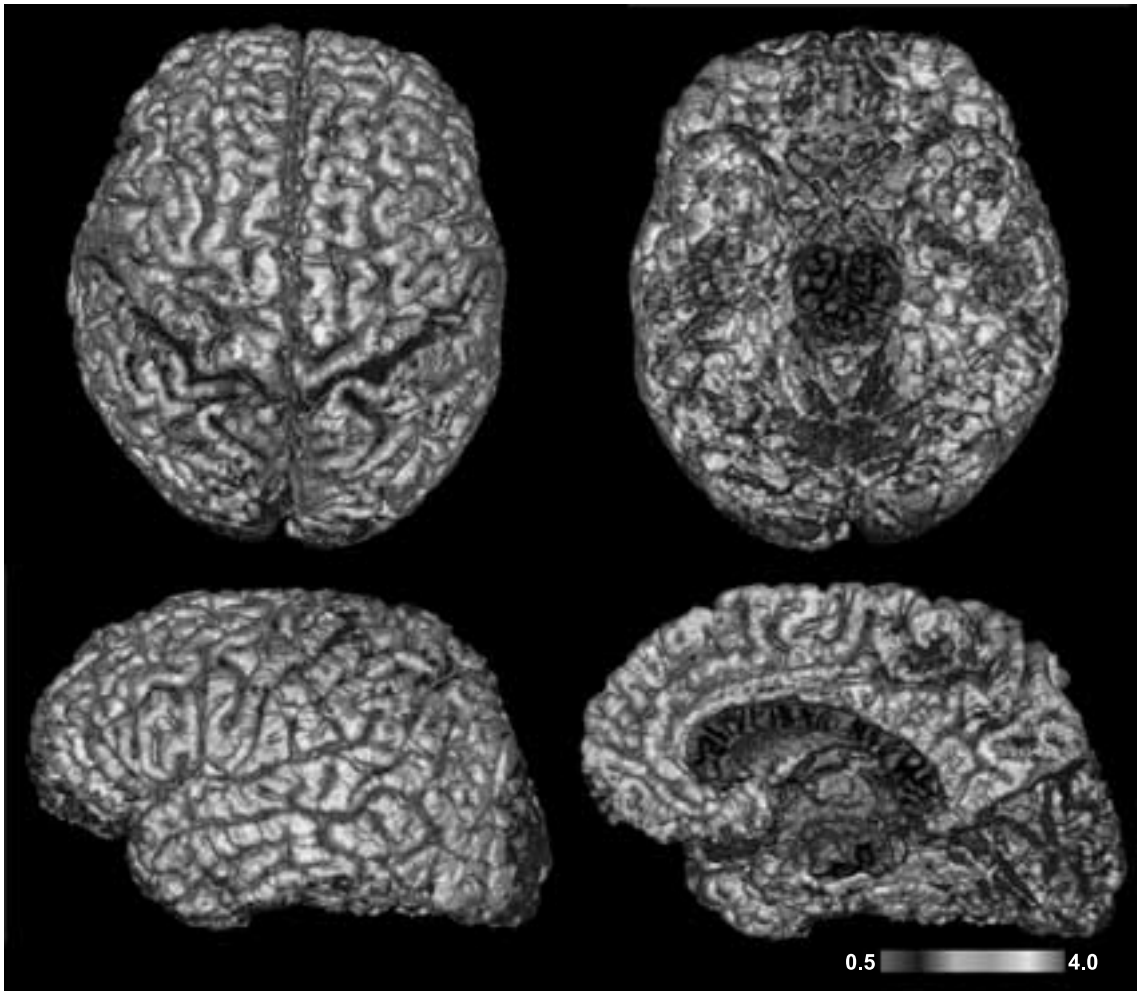

Figure 3. Cortical thickness (in mm) mapped onto the grey matter surface of a normal subject, reconstructed from top (top), and left (below). Note that the cortex is thicker in the frontal and temporal lobe (≈2.5 mm), in comparison with the motor and the visual cortex (≈1.7 mm).

Sulcal Substructure	Normal Subject		Patient	
	left	right	left	right
Superior frontal sulcus, posterior part	2.437±0.481	2.377±0.503	1.314±0.260	1.425±0.256
Central sulcus, inferior part	1.544±0.518	1.617±0.581	1.232±0.188	1.220±0.249
Middle frontal sulcus, middle part	2.483±0.495	2.479±0.444	1.370±0.345	1.319±0.261
Intraparietal sulcus	2.402±0.524	2.359±0.450	1.500±0.500	1.381±0.330
Superior temporal sulcus, middle part	2.235±0.452	2.680±0.436	1.628±0.499	1.464±0.451
Calcarine sulcus, posterior part	1.586±0.505	1.754±0.474	1.338±0.631	1.291±0.613

Table 1. Mean and variance of cortical thickness (in mm) from the cortical banks adjacent to the named example sulcal subregions. Except for the visual cortex, an atrophy of 60% was noted in the example patient.

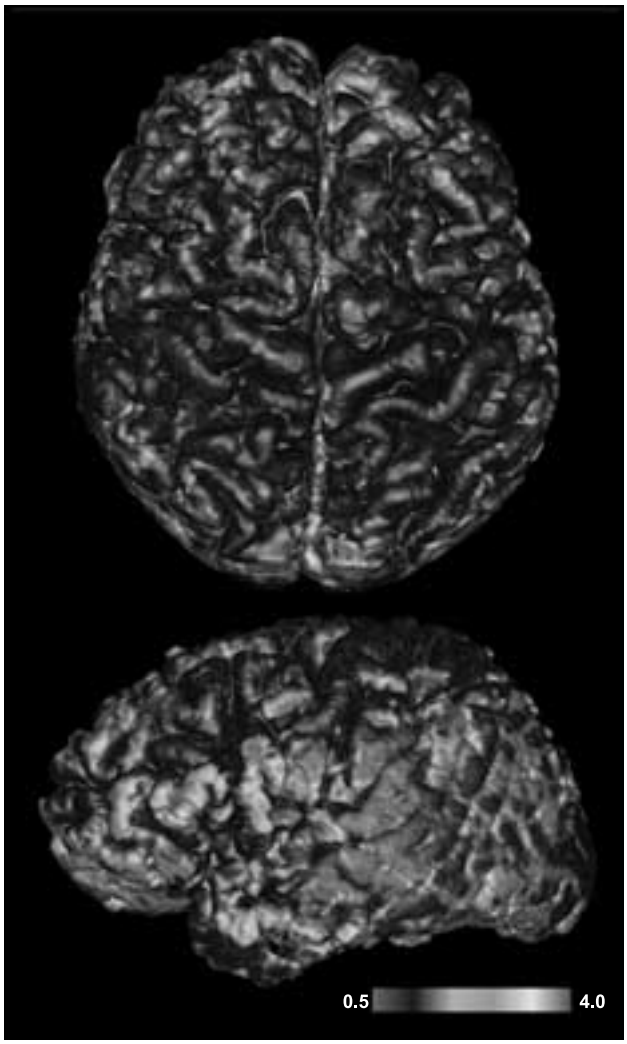

Figure 4. Cortical thickness (in mm) mapped onto the grey matter surface of a patient suffering from Alzheimer's disease, reconstructed from top (top), and left (below). In comparison with the normal subject (see Fig. 4), the cortex is generally thin ($\approx$1.5 mm), especially in fronto-temporal parts of the brain, where a white matter atrophy was noted as well. The cortical atrophy was more prominent at crowns, whereas the cortical thickness at fundi was similar to the normal subject.

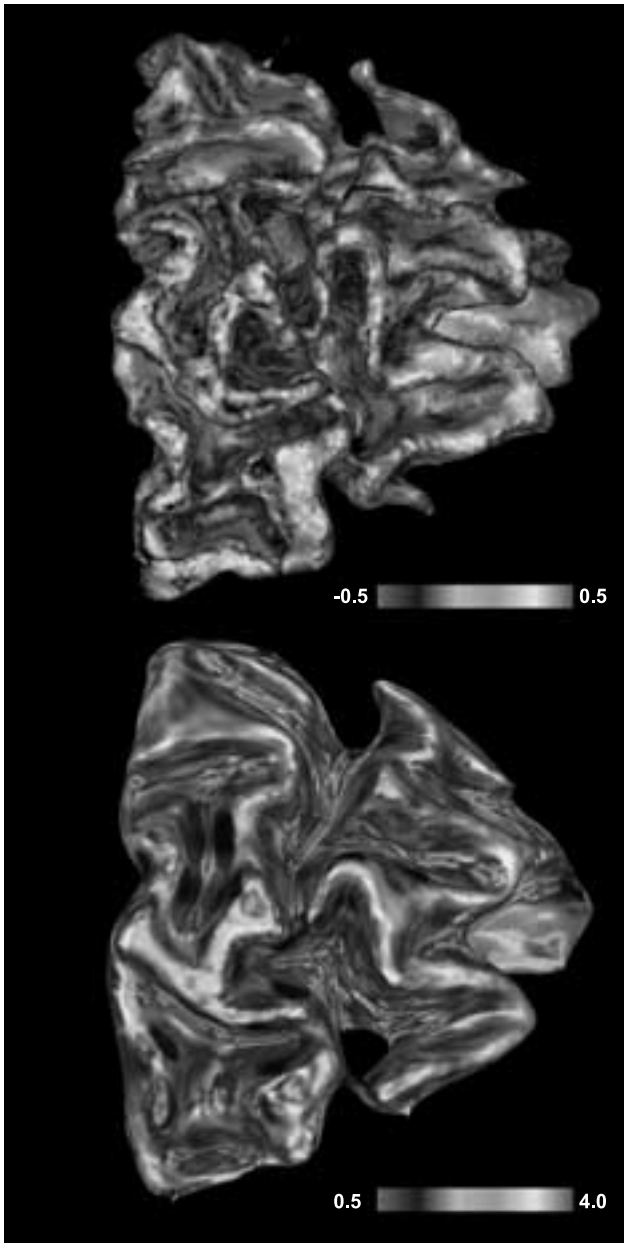

Figure 5. Top: Patch from the right frontal lobe of the normal subject. The mean curvature of the white matter surface was color-mapped onto the surface. Magenta corresponds to concave (i.e. fundi), red to convex areas (i.e. gyral crowns). Below: Cortical thickness (in mm) mapped onto the grey matter surface of the same patch. Sulci were unfolded in order to expose fundi. By comparison, the cortex is generally thicker at gyral crowns in comparison with fundi.

0-7695-0737-9/00 $10.00 (c) 2000 IEEE

Fig. 6 shows a plot of the cortical thickness as a function of the local curvature, which confirmed the qualitative finding above. Interestingly, the patient's cortex at fundi appeared to have normal thickness measurement, thus, the atrophy may affect crown regions only. Of course, more cases need to be studied before final conclusions may be drawn.

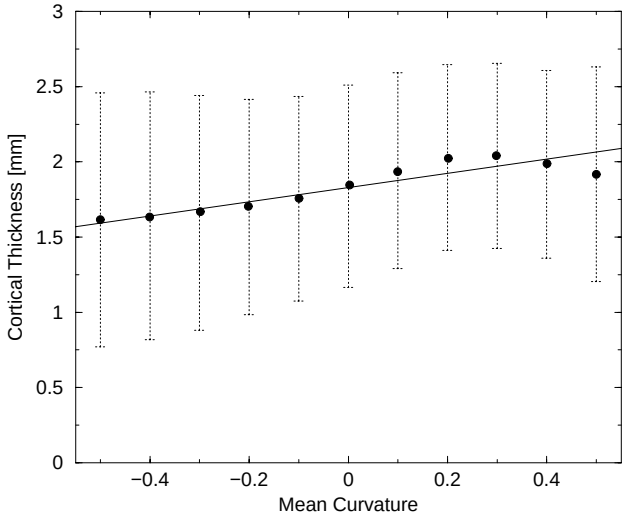

Figure 6. Mean and variance of the cortical thickness as a function of the curvature, as determined from the same patch as in Fig. 5. The cortex is thicker at convex areas (typically at gyral crowns) in comparison with concave areas (fundi). Regression line: 1.85+0.66x, r^2=0.0225, p=0.

4. Discussion

The focus of this study was to develop a reliable segmentation procedure for the neocortex as revealed by single-channel MR data sets of the human head. This procedure may be called automatical in a sense that no operator interaction is required except for the initial alignment step. The only sensible settings are the WM and GM limits, which define the boundary of the GM compartment. While a simple assignment based on the class probabilities in the initial segmentation appears attractive and plausible, more data sets need to be analyzed in order to confirm this suggestion. An efficient layout of the data structures and careful optimization of the algorithms ensured a satisfying performance even for large meshes (>1000 k vertices). If such non-optimized meshes are studied, the whole procedure needed less than 3 h computation time (R10K processor at 195 MHz).

A few caveats: The intensity correction scheme exerts a critical influence on thickness results in certain areas, and more cross-checking with histological results is necessary to ensure reliable results for the whole brain. Small areas of high thickness values ("red spots" in Fig. 3) often correspond to segmentation errors, where structures adjacent to or connected with the brain (e.g., meninges and vessels) are assigned to the grey matter compartment. The simple region selection scheme applied here needs revision, because a consistent region labelling must be introduced when studying groups.

Elaborate schemes for grey matter segmentation were developed by Xu *et al.* [21]. However, they acheive a segmentation of the *central layer* of the GM, and it may be hard to derive a measure for the cortical thickness from their segmentation. The only study that used image processing methods to derive thickness measurements in vivo was conducted by Magnotta *et al.* [9]. Although they report results from a large number of cases, they segment the GM-WM boundary and the central GM layer, and *double* measured values to obtain the cortical thickness. Given the uncertainity of defining a central GM layer and the necessary symmetry assumption, we regard this approach as questionable. An interesting alternative to our approach was developed by Zeng *et al.* [22], who used a level-set method with coupled surfaces to segment both boundaries in a single step. Their reported coupling constraint of 2.4-3.6 mm surface distance appears too narrow on the basis of the results obtained here.

Neurobiologically even more interesting is the regional cortical volume, which is easily derived from the regional thickness measurements. The intent of this research is to provide a framework for the quantitative morphometric description of disease processes in the brain. The grey matter segmentation scheme proposed here forms a significant building block within such a framework.

Acknowledgments

The authors would like to thank D.L. Pham for advice in implementing their imhomogeneity correction scheme. Data sets for this study were kindly provided by D. Norris (MPI) and H.J. Gertz (Dept. of Psychiatry, University Hospital, Leipzig).

References

[1] Blinkov SM, Glezer II (1968) *The Human Brain in Figures and Tables. A Quantitative Handbook.* Plenum Press, New York.

[2] A.M. Dale, M.I. Sereno. Improved localization of cortical activity by combining EEG and MEG with MRI cortical surface reconstruction: a linear approach. *Journal of Cognitive Neuroscience* 5:162-176, 1993.

[3] D. Eberly. Distance between point and triangle in 3D. `http://www.magic-software.com /graphics/src/dist/pt3tri3.pdf`, 1999.

[4] J. Gomes, O. Faugeras. Segmentation of the inner and outer surfaces of the cortex in man and monkey: an approach based on partial differential equations. *NeuroImage* 6:152, 1999.

[5] A. Gueziec, R. Hummel. The wrapper algorithm: surface extraction and simplification. In *Workshop on Biomedical Image Analysis (Seattle),* pp. 204-213. IEEE Computer Press, Los Alamitos, 1994.

[6] D.G. Kendall, K. Barden, T.K. Carne. *Shape and Shape Theory.* Wiley, Chichester, 1999.

[7] F. Kruggel, D.Y. von Cramon. Alignment of magnetic-resonance brain datasets with the stereotactical coordinate system. *Medical Image Analysis* 3:1-11, 1999.

[8] G. Lohmann, D.Y. von Cramon. Sulcal basins and sulcal string as new concepts for describing the human cortical topography. In *Workshop on Biomedical Image Analysis (Santa Barbara),* pp. 24-33. IEEE Press, Los Alamitos, 1998.

[9] V.A. Magnotta, N.C. Andreasen, S.K. Schultz, G. Harris, T. Cizadlo, D. Heckel, P. Nopoulos, M. Flaum. Quantitative in vivo measurement of gyrification in the human brain: changes associated with aging. *Cerebral Cortex* 9:151-160, 1999.

[10] B.A. Payne, A.W. Toga. Surface mapping of brain function on 3D models. *IEEE Computer Graphics and Applications* 10:33-41, 1990.

[11] D.L. Pham, J.L. Prince. An adaptive fuzzy segmentation algorithm for three-dimensional magnetic resonance images. In *Information Processing in Medical Imaging (IPMI'99), Lecture Notes in Computer Science* Vol. 1613, pp. 140-153. Springer, Heidelberg, 1999.

[12] G. Rajkowska, P.S. Goldman-Rakic. Cytoarchitectonic definition of prefrontal areas in the normal human cortex: I. Remapping of areas 9 and 46 using quantitative criteria. *Cerebral Cortex* 5:307-322, 1995.

[13] A. Sotrel, P.A. Paskevich, D.K. Kiely, E.D. Bird, R.S. Williams, R.H. Myers. Morphometric analysis of the preforntal cortex in Huntington's disease. *Neurology* 41:1117-1123, 1991.

[14] E.M. Stokeley, S.Y. Wu. Surface parameterization and curvature measurement of arbitrary 3-D objects: five practical methods. *IEEE Transactions on Pattern Analysis and Machine Intelligence* 14:833-840, 1991.

[15] R.D. Terry, A. Peck, R. DeTeresa, R. Schechter, D.S. Horoupian. Some morphometric aspects of the brain senile dementia of the Alzheimer type. *Annals of Neurology* 10:184-192, 1981.

[16] R.D. Terry, R. DeTeresa, L.A. Hansen. Neocortical cell counts in normal human adult aging. *Annals of Neurology* 21:530-539, 1986.

[17] D. Terzopoulus, K. Fleischer. Deformable models. *The Visual Computer* 4:306-331, 1988.

[18] P. Thevenaz, T. Blu, M. Unser. Image Interpolation and resampling. In *Handbook of Medical Image Processing.* IEEE Press, Los Alamitos, 1999.

[19] W. Welker. Why does cerebral cortex fissure and fold? A review of determinants of gyri and sulci. In *Cerebral Cortex* Vol. 8b, pp. 3-136. Plenum Press, New York, 1996.

[20] C. Xu, J.L. Prince. Snakes, shapes, and gradient vector flow. *IEEE Transactions on Image Processing* 1998:359-369.

[21] C. Xu, D.L. Pham, R.E. Rettmann, D.N. Yu, J.L. Prince. Reconstruction of the human cerebral cortex from magnetic resonance images. *IEEE Transactions on Medical Imaging* 18:467-480, 1999.

[22] X. Zeng, L.H. Staib, R.T. Schultz, J.S. Duncan. Volumetric layer segmentation using coupled surfaces propagation. In *Computer Vision and Pattern Recognition (CVPR'98),* pp. 708-715. IEEE Press, Los Alamitos, 1998.

[23] K. Zilles, R. Werners, U. Busching, A. Schleicher. Ontogenesis of the laminar structure in areas 17 and 18 of the human visual cortex. A quantitative study. *Anatomy and Embryology* 174:339-353, 1986.